



HHS Public Access

Author manuscript

ACS Nano. Author manuscript; available in PMC 2018 February 12.

Published in final edited form as:

ACS Nano. 2015 ; 9(4): 3780–3790. doi:10.1021/nn5066028.

Controlling Differentiation of Adipose-Derived Stem Cells Using Combinatorial Graphene Hybrid-Pattern Arrays

Tae-Hyung Kim^{†,||,#}, Shreyas Shah^{†,#}, Letao Yang[†], Perry T. Yin[‡], Md. Khaled Hossain[⊥], Brian Conley[§], Jeong-Woo Choi^{*,||,⊥}, and Ki-Bum Lee^{†,‡,*}

[†]Department of Chemistry and Chemical Biology, Rutgers, The State University of New Jersey, 610 Taylor Road, Piscataway, New Jersey 08854, United States

[‡]Department of Biomedical Engineering, Rutgers, The State University of New Jersey, 599 Taylor Road, Piscataway, New Jersey 08854, United States

[§]Department of Cell Biology and Neuroscience, Rutgers, The State University of New Jersey, 604 Allison Road, Piscataway, New Jersey 08854, United States

^{||}Department of Chemical & Biomolecular Engineering, Sogang University 35 Baekbeom-ro, Mapo-gu, Seoul 121-742, Republic of Korea

[⊥]Interdisciplinary Program of Integrated Biotechnology, Sogang University, 35 Baekbeom-ro, Mapo-gu, Seoul 121-742, Republic of Korea

Abstract

Control of stem cell fate by modulating biophysical cues (*e.g.*, micropatterns, nanopatterns, elasticity and porosity of the substrates) has emerged as an attractive approach in stem cell-based research. Here, we report a method for fabricating combinatorial patterns of graphene oxide (GO) to effectively control the differentiation of human adipose-derived mesenchymal stem cells (hADMSCs). In particular, GO line patterns were highly effective for modulating the morphology of hADMSCs, resulting in enhanced differentiation of hADMSCs into osteoblasts. Moreover, by generating GO grid patterns, we demonstrate the highly efficient conversion of mesodermal stem cells to ectodermal neuronal cells (conversion efficiency = 30%), due to the ability of the grid patterns to mimic interconnected/elongated neuronal networks. This work provides an early demonstration of developing combinatorial graphene hybrid-pattern arrays for the control of stem cell differentiation, which can potentially lead to more effective stem cell-based treatment of incurable diseases/disorders.

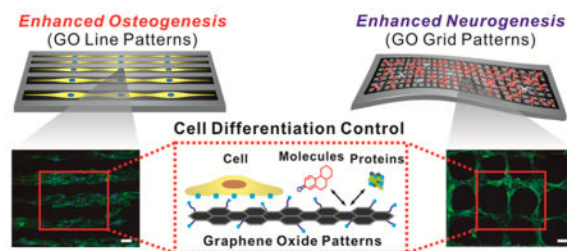
*Address correspondence to: jwchoi@sogang.ac.kr, kblee@chem.rutgers.edu.

#These authors contributed equally to this work.

Conflict of Interest: The authors declare no competing financial interest.

Supporting Information Available: Experimental details and additional figures including characterization of NGO and NGO combinatorial patterns, helium ion microscopic (HIM) images of small-sized NGO grid patterns, NGO square patterns on tissue culture plate analyzed by confocal Raman spectroscopy, confocal Raman mapping of NGO line patterns on gold substrate, AFM image of NGO square pattern on gold substrate, Raman spectroscopy after ultrasonic cleaning of NGO patterns, actin-stained images of hADMSCs on glass, gold, NGO-coated gold, NGO line and NGO grid patterns, comparison of hADMSC osteogenesis on different substrates, size-dependent effect of NGO line patterns on osteogenesis of hADMSCs and neuronal differentiation of hADMSCs on laminin (LN)-coated substrates. This material is available free of charge *via* the Internet at <http://pubs.acs.org>.

Graphical abstract



Keywords

graphene arrays; combinatorial pattern; cell morphology; adipose-derived stem cells; differentiation

In the past decade, advances in stem cell technologies have significantly transformed the scientific and clinical approaches used to develop effective therapies.^{1–9} Owing to the intrinsic ability of stem cells to self-renew and differentiate into practically any given cell type, stem cells have the potential to treat numerous diseases and injuries found throughout the body.¹⁰ However, the highly efficient differentiation of stem cells into specific cell-types of interest (*e.g.*, bone, neurons, pancreatic cells, *etc.*) remains a major obstacle for the advent of regenerative medicine. In particular, while the conventional paradigm that is applied to selectively guide stem cell fate has been the use of precisely defined media conditions and/or the controlled delivery of small molecules and genetic factors, a myriad of recent findings implicate that biophysical cues also play a critical role in this process, warranting further investigation into this area.^{1,11,12}

Biophysical cues, which encompass the topographical and mechanical properties that are imposed by the microenvironment on the cell, act through cell–substrate interactions to alter upstream cytoskeletal dynamics and downstream gene expression, which can ultimately modulate cellular behaviors such as differentiation.^{3,13–16} As a means to systematically control the biophysical microenvironment of cells, nano- and microstructures/patterns have emerged as an interesting approach to direct stem cell differentiation without the need for any genetic modification and/or external stimulation.^{15,17,18} For example, it has been shown that micropatterns, ranging on the scale of a few micrometers to a hundred micrometers, are effective in steering stem cell fate. In particular, this strategy entails manipulating the cellular morphology by using ECM proteins arranged in geometric orientations that can mimic the cellular arrangements found in the native tissues. Compared to nonpatterned substrates such as tissue culture plates, highly efficient tissue-specific stem cell differentiation has been demonstrated using this method, including: cell–cell contact on network-like grid patterns for neuronal differentiation,^{15,19} reduced traction forces on square patterns for adipogenic differentiation^{20,21} and elongated morphology on line patterns for myocardial²² and osteogenic differentiation.^{12,17}

In addition to modulating the cell shape and orientation using combinatorial patterns, the use of biomaterials with unique topographical features, which can exist in the form of micro/

nano-architecture, for stem cell culture has also exhibited exceptional effects on stem cell behavior.^{18,23–25} Among the multitude of materials available, graphene-based nanomaterials, such as graphene oxide (GO), have been increasingly investigated. Numerous studies have demonstrated that the culture of stem cells on GO can efficiently steer stem cell differentiation *via* distinct physico-chemical characteristics of GO including amphiphilicity, the honeycomb carbon structure, and different surface chemistries ($-C-O-C$, $C-O-H$, $-COOH$, *etc.*).^{26,27} For instance, the osteogenesis,^{26,28} adipogenesis,²⁶ neurogenesis²⁹ and oligodendrogenesis³⁰ of tissue-derived stem cells were found to be enhanced by the distinct features of GO, which affected cell spreading and morphology. GO was also found to affect the absorption of biomolecules, which is otherwise difficult to achieve using other types of ECM and/or carbon-based nanomaterials. Up until now, the coating of various substrates (*e.g.*, glass, polymers, nanofibers) with GO has been primarily achieved by bulk deposition methods. However, this method imparts little to no control over the orientation and arrangement of GO on the target surface. As a result, there is significant room for improvement, especially in regard to specifically controlling the modulation of stem cell differentiation using GO.

Given the significant role that patterned geometries have on specifically guiding stem cell differentiation, we hypothesize that the fabrication of combinatorial geometries that are composed of graphene-based nanomaterials can allow for the combination of the advantages offered by both approaches to more precisely guide stem cell differentiation. In particular, by generating graphene-based combinatorial patterns, stem cell differentiation can be controlled by (1) modulating cellular morphology by varying GO patterns, (2) introducing nanotopography from GO to alter/enhance cell adhesion, and (3) promoting interactions between small molecules/proteins and the surface of GO. Such an approach exploits the excellent material properties of graphene, while potentially enhancing the efficiency with which we can modulate stem cell behavior/differentiation by combining with micropatterns.

To this end, we report a novel strategy to guide stem cell differentiation into specific cell lineages by employing combinatorial GO hybrid-patterns of specific geometries (Figure 1). As a model stem cell line, we selected human adipose-derived mesenchymal stem cells (hADMSCs), which have the capability to differentiate into a number of cell lineages including fat, bone, cartilage, and neural cells.^{31,32} Among the varying micropatterned geometries of nanosized GO (NGO) that were utilized for hADMSC culture, we observed that the hADMSCs adopted an elongated morphology on NGO line patterns, which resulted in highly enhanced osteogenic differentiation. On the other hand, NGO grid patterns were observed to successfully differentiate the mesodermal cells (hADMSCs) to ectodermal cells (neuron), which is traditionally considered to be extremely difficult to achieve even using conventional differentiation protocols. In this way, we demonstrated that guiding stem cell differentiation using combinatorial graphene hybrid-pattern arrays is an attractive approach that has immense potential for regenerative medicine.

RESULTS AND DISCUSSION

Generation of Graphene Combinatorial Patterns with Different Geometries

To generate large areas of combinatorial NGO patterns for our studies, we utilized a microcontact printing (MCP) method. In particular, MCP is a very simple and robust technology, allowing for the generation of combinatorial patterns over large surface areas that are ideal for cell culture.³³ For this purpose, NGO was first synthesized using a modified Hummer's method.³⁴ Briefly, to make highly oxidized NGO, the amount of graphite as a starting material was decreased from 3 to 1 g in conjunction with the increase of time for stirring in sulfuric acid from 3 to 8 h. The size of GO was then adjusted to be around 100 nm by an additional filtration process. The physicochemical properties of these NGO were determined using transmission electron microscopy (TEM) (Figure 2a,i), dynamic light scattering (DLS) (Figure 2a,ii), zeta potential (Figure 2a,iii), XPS analysis (Figure 2a,iv) and Raman spectra of NGO (Supporting Information Figure 1). From our characterization, we determined that the NGO was highly negatively charged with many hydroxyl groups (highly hydrophilic) and had a size of around 100 nm. On the other hand, for the generation of NGO patterns, there are many critical factors that affect the quality of the resulting NGO patterns, including the oxidization level (hydrophilicity), size and concentration of NGO, solvent for NGO dispersion, parameters for spin coating (*e.g.*, spin speed, acceleration, spin time), humidity, temperature, force applied to the stamp (M), and the time needed for stamping. The highly oxidized (C:O = 6:4) nature of the NGO was found to be critical for the attachment of the NGO films onto the desired substrates, which occurred *via* strong hydrophilic–hydrophilic interaction. To this end, we generate highly stable and homogeneous NGO films by first depositing NGO solution on the micropattern-bearing PDMS stamps (rendered hydrophilic by oxygen plasma treatment prior to NGO deposition). Specifically, during the stamping process, the PDMS slowly recovers its initial highly hydrophobic state, thereby weakening the interaction between the NGO film and the PDMS. This results in the transfer of NGO from the surface of PDMS to the desired substrate. For instance, oxygen plasma-treated gold substrate were first used to attract hydrophilic NGO film on the PDMS stamp. The force applied to PDMS during the stamping process, as well as the humidity, contributed to the strong attachment of NGO on the surface. By applying an optimized force (0.79 N) under a high humidity level for 40 min, we were able to generate highly stable NGO combinatorial patterns, without the use of additional chemical linkers or other complex processes. As a result, NGO patterns with different sizes (5–50 μm) and shapes (squares, lines, grids, specific character) were successfully generated on the gold surface (Figure 2b,c). Remarkably, the size of the NGO pattern could be reduced to around 1.5 μm without sacrificing the quality of structure (Supporting Information Figure 2).

Generation of Graphene Combinatorial Patterns on Different Substrates

While the generation of high quality graph-ene combinatorial patterns on gold surfaces is suitable for cell culture, it would be highly advantageous to expand this process to other types of biocompatible surfaces. As such, tissue culture plates (TCP), flexible PDMS polymer, and biodegradable poly(lactic-*co*-glycolic acid) (PLGA) were chosen for the generation of NGO combinatorial patterns, since these types of substrates not only have

potential for large scale *in vitro* studies (TCP), but also possess huge potential for *in vivo* transplantation (PDMS, PLGA) (Figure 3a). NGO patterns having dimensions of 10 and 20 μm were both successfully generated on glass/Au, TCP, highly flexible PDMS substrates, and PLGA biodegradable film, as observed using helium ion microscopy (HIM) (Figure 3b). Confocal Raman mapping was further used to confirm the chemical and structural characteristics of the NGO combinatorial patterns (Figure 3c). We observed that only areas covered by NGO exhibited strong Raman intensity at the location of the distinct D (1350 cm^{-1}) and G (1580 cm^{-1}) peaks of GO, which concurs with the images acquired from HIM and AFM (Supporting Information Figures 3 and 4). Efficient NGO patterns generated with different geometries on common TCP were also confirmed using confocal Raman mapping (Supporting Information Figure 5). Moreover, the patterns generated on these surfaces were found to be extremely stable with negligible removal of NGO even under severe washing conditions (acetone, DIW and ethanol washing for 15 min each with sonication) (Supporting Information Figure 6). This long-term stability is highly important as it prevents possible adverse effects such as the release of NGO from the surface while stem cell cultured on the substrate of being differentiated. In addition, this long-term stability facilitates the stable interaction of the ECM environment with stem cells over extended periods of time, which is required during differentiation (at least 2–3 weeks for the total differentiation process).¹⁹

Investigation of the Functions of Morphological Cue on the Osteogenic Differentiation of hADMSCs

After successful pattern generation, hADMSCs were cultured on the NGO patterned substrate to modulate their cellular morphology. A thiol-modified passivation molecule (HS-C₁₁-PEG₄-OH) was used prior to the cell seeding to prevent cell adhesion to areas of the substrate that lack NGO, which is critical for the NGO pattern-mediated manipulation of cell morphology.¹⁵ In this way, the morphology of the hADMSCs was successfully altered, solely based on the geometry of the underlying NGO micropatterns (Supporting Information Figure 7). In particular, we observed that cell spreading was the highest on NGO line patterns. Owing to the fact that cell spreading, in combination with elongated morphology, has been previously found to be important for osteogenesis,³⁵ we next sought to initiate osteogenesis of hADMSCs grown on NGO line patterns.

Toward this objective, hADMSCs that were grown on NGO line pattern for 2 days were treated with osteogenic medium (OM). Remarkably, the NGO line patterns were stable and remained on the gold surface even after 3 weeks of incubation, which contributed to maintaining elongated morphologies of hADMSCs (Figure 4a). The differentiation of hADMSCs into the osteoblasts was confirmed by three distinct methods: alkaline phosphatase assay (preosteogenic marker),³⁶ immunostaining (osteocalcin-the marker of osteoblast),²⁸ and Alizarin red S assay (level of calcification).^{26,28} Specifically, all cells treated with OM showed the expression of osteocalcin regardless of the type of substrate employed for osteogenesis (Figure 4b). However, hADMSCs on the NGO line pattern were found to follow the direction and geometry of the NGO pattern, resulting in the enhanced expression of osteocalcin, which was largely due to their elongated/aligned morphology,¹² the increased cell spreading³⁷ and the physicochemical properties of GO.²⁶ Next, the level of calcification levels, which is the most important indicator for bone regeneration, was

confirmed by Alizarin red S assay, which selectively stains for calcium generated by osteoblasts. We observed that hADMSCs grown on the NGO line pattern showed enhanced levels of calcification (*shown in red*), while cells grown on bare Au and NGO-coated substrates failed to show remarkable enhancement of calcification (Figure 4c). Interestingly, the NGO-coated control substrates showed uniformly distributed calcium expression with universally low levels of calcification (weak intensities of Alizarin red S), which was clearly distinguishable from NGO line pattern. This proves that there were distinct synergistic effects that were caused by culturing the ADMSCs on the NGO line pattern thereby enhancing the osteogenesis of hADMSCs (Figure 4c). Finally, quantification of osteogenesis of hADMSCs by extraction with cetylpyridinium chloride (CPC) further confirmed the increased levels of calcification of cells on the NGO line pattern, which was 54.5% and 41% higher than that of bare Au and NGO-coated substrate, respectively (Figure 4e). These results were found to match the preosteogenic marker (AP) staining at day 14, which showed a slight increase in AP expression in cells cultured on the NGO line pattern when compared to the cells on bare Au and uniform NGO-coated substrate (Figure 4d). Since calcification normally occurs after 2 weeks of differentiation, it seemed that the enhanced osteogenic differentiation of hADMSCs, which was confirmed by AP assay, contributed to the increased activity of osteoblast mineralization, resulting in the remarkable enhancement of calcification between weeks 2 and 3 of differentiation. We further compared the activity of osteoblast mineralization on protein-patterned substrates (without NGO) *via* MCP techniques using 1-octadecanethiol (ODT) as an ink molecule. Even though cells on fibronectin (FN) protein patterns showed enhanced calcification level compared to the substrate with or without FN coating, cells grown NGO line patterns showed the highest calcification level compared to the other groups (Supporting Information Figure 8). This indicates that the combination of NGO and micropatterns was essential for promoting osteogenesis of hADMSCs. Next, we attempted to confirm the size-dependent effects of NGO pattern on the osteogenesis. The hADMSCs were found to follow NGO line patterns, showing different morphologies as sizes of NGO patterns and gap distances were varied (Supporting Information Figure 9). On the basis of HIM images, small NGO patterns with narrow gap distance were found to generate patterned hADMSCs with partially disoriented and interconnected morphology, especially for 10 μm NGO pattern with 5 μm gap distance, while large NGO patterns with wide gap distance were found to generate well-oriented and noninterconnected morphologies. In terms of osteogenesis of hADMSCs, 30 μm NGO line pattern with 15 μm gap showing both well-oriented and partially interconnected morphology was found to be the best for the differentiation, based on calcification results determined by Alizarin red S assay. Hence, based on the results, we could conclude that the NGO line pattern had distinct effects that steered the differentiation of hADMSCs toward the osteoblast lineage.

Additionally, since the strong effects of NGO line pattern on the osteogenesis of hADMSCs were successfully confirmed, we attempted to extend the potential of the developed technique by fabricating a patch-like material (Bone-patch). This material is composed of highly flexible PDMS polymer (Young's modulus: 6.2 MPa) that was 6.5 times more flexible than normal PDMS (supporting layer), NGO line pattern (cell adhesion and differentiation) and the differentiated osteoblasts (bone healing), which could be useful for

further *in vivo* applications of hADMSCs (Figure 4f). The fabricated material was transparent, nontoxic, and highly flexible, while allowing for the maintenance of cell attachment even after several instances of bending were applied (Figure 4g). We observed that the osteocalcin expression was enhanced in cells on both the NGO film and NGO line pattern after differentiation (Figure 4h), similar to the cells grown on rigid substrate (Figure 4b). Moreover, the hADMSCs grown on the NGO line pattern/polymer complex showed enhanced levels of calcification compared to both bare and NGO-coated polymer, which is highly important for treating bone defects (Figure 4h). This is quite remarkable due to the practical use of proposed bone-patch for the bone regeneration.

Enhanced Neuronal Differentiation of hADMSCs Using Graphene-Hybrid Grid Patterns

Subtle changes in the physical microenvironment, such as changes in the substrate stiffness, topography, ligand display, and ECM composition/shape, have been reported to significantly alter stem cell differentiation in both mesenchymal and neural stem cells.^{1,38} For instance, ECM micropatterns have previously been shown to influence NSC fate, wherein square patterns promoted glial cell formation and grid patterns promoted neuronal cell formation.¹⁵ At the same time, changes in graphene properties have been seen to influence both mesenchymal differentiation (*e.g.*, bone, fat, heart) and neural differentiation (*e.g.*, neuron, oligodendrocyte).^{26,28–30,39–41} As such, while we have provided strong evidence demonstrating the enhanced osteogenic differentiation of hADMSCs on NGO line patterns, we next sought to investigate the potential of altering the combinatorial NGO pattern-arrays to achieve neuronal differentiation of hADMSCs, which has been considered to be challenging since it entails a conversion from mesoderm to ectoderm (Figure 5).^{42,43} To achieve neuronal differentiation, we selected to generate NGO grid hybrid patterns, as the geometry of grid pattern mimics the morphologies of neurons *in vivo*, which are elongated and interconnected, and may enhance neuron formation and the electrical signaling of neural networks.^{15,44,45} Prior to seeding cells on NGO substrates, hADMSCs were primed for neural differentiation using precise media formulations with growth factors and media changes. Thereafter, neural-induced hADMSCs were seeded on various substrates including PLL-coated Au (conventional substrate for *in vitro* neural cultures), NGO-coated Au, and NGO grid-patterned substrates, wherein all of the substrates were coated with laminin to facilitate cell adhesion. It was observed that the neural-induced hADMSCs attached and spread well on all substrates, wherein the NGO patterned substrates were seen to permit a network-like formation by Day 5 (Figure 5a). Upon further monitoring, distinct changes in cellular morphology were evident by Day 10. While cells grown on the Au surface exhibited a more circular morphology, cells grown on the NGO grid patterns were characterized by a bipolar orientation and pervasive cellular extensions (Figure 5a,b). Quantification of the length of the cellular extensions revealed that the NGO-coating promoted higher degrees of outgrowth, when compared to the control substrates (Figure 5c). The number of cells exhibiting processes (neurites) and the extent of neurite growth are typical quantitative measurements indicative of neuronal differentiation.⁴⁶ Immunostaining for the neuronal marker TuJ1 further confirmed the enhanced differentiation, in which cells grown on NGO grid patterns showed a significantly higher percentage of cells expressing TuJ1 (~30%) compared to PLL-coated Au (~8%) and NGO-coated Au (~15%) (Figure 5d). We further compared the degree of neuronal differentiation to laminin-patterned substrates (without

NGO), using ODT as an ink molecule for MCP. While greater number of cells expressing TuJ1 were found on the laminin-patterned grid substrates compared to control substrates, the NGO grid patterns resulted in the highest percentage of TuJ1 expressing cells (Supporting Information Figure 10). This indicates that the combination of NGO and micropatterns was essential for promoting neurogenesis of hADMSCs. In this way, we demonstrated the potential of our GO hybrid-patterns to guide hADMSC neuronal differentiation, underscoring the scope of our platform for stem cell culture and differentiation.

CONCLUSION

Overall, we have developed novel NGO patterns, which were highly effective for controlling the differentiation of hADMSCs directly derived from patients (29- and 63-year-old-females). The NGO combinatorial pattern-arrays, with different sizes and geometries, were successfully generated on various kinds of cell-compatible substrates including Au-coated cover glass, cell culture dish, flexible PDMS and even biodegradable PLGA film, without the use of any chemical linkers and/or additional processes. In addition, we found that the morphology of hADMSCs could be effectively manipulated by NGO micropatterns, while maintaining its structure for more than a month. The NGO line patterns, generated on both rigid gold substrates and flexible polymers, were found to be effective for guiding osteogenic differentiation of hADMSCs. The physicochemical properties of NGO and the combinatorial pattern geometry contributed to an elongated and well-spread morphology of the attached hADMSCs, leading to 54.5% and 41% higher differentiation efficiency of hADMSCs into osteoblasts compared to gold without NGO and NGO film-coated gold substrates, respectively. Even though graphene is more preferable than GO to generate osteoblasts from MSCs, the reduction process was not used in this study to prevent possible absorption of toxic chemicals, which are required for reduction,⁴⁷ as well as to avoid damage to polymeric/biodegradable substrates, which may harm the potential of developed NGO-patterning techniques. Moreover, by generating NGO grid patterns that mimic elongated and interconnected neuronal network combined with the positive effects of GO on neurogenesis, we reached a conversion ratio of MSCs to neurons of up to 30%, which has never been reported before using any other current methods. This is quite remarkable, since the enhanced neuronal differentiation of hADMSCs may pave the way to use these readily available cell types for regenerative medicine, which could be useful for treating serious neurological disorders and diseases including spinal cord injury and/or Parkinson's disease.^{42,43}

The long-term stability of NGO micropatterns, which can be generated on practically any kind of substrate, makes our approach attractive for various kinds of biomedical applications. For instance, our approach can be used for the mass production of patient-specific cells using NGO-patterned cell culture wares and biodegradable hydrogels with NGO patterns on their surfaces. Additionally, since the elasticity of the substrate is known to be a key factor for guiding the differentiation of stem cells into specific lineages *via* mechanotransductive pathways,^{1,48,49} the strategy introduced here can be further applied to generate NGO combinatorial patterns on elasticity-controlled polymer substrates, which could synergistically steer stem cell differentiation in a more efficient manner. Hence, the

platform developed in this study can serve as a powerful and general tool for the development of future cell type- and patient-specific stem cell-based therapies.

METHODS

Synthesis of Highly Oxidized Nano Graphene Oxide (NGO)

Graphene oxide was synthesized based on a modified Hummers method;³⁴ 1.0 g of graphite, 2.5 g of $K_2S_2O_8$, and 2.5 g of P_2O_5 were carefully added into 12 mL of concentrated H_2SO_4 solution and the mixture was stirred at 80 °C for 7 h to achieve preoxidized graphite. Afterward, the preoxidized graphite was washed, filtered out and dried. The powder was then slowly added into 12.0 mL of H_2SO_4 together with 15 g of $KMnO_4$ in an ice bath while stirring the mixture at 35 °C for 3 h. Then, 250 mL of distilled water was further added, the solution was stirred for 2 h, and 700 mL of distilled water and 20 mL 30% H_2O_2 solution were added to finalize the reactions, showing a bright yellow color. The solution containing graphene oxide flakes was filtered out using 0.2 μm filter, followed by 2 h of ultrasonication. After centrifugation of the solution at 10 000 rpm for 30 min, the suspension with single or few-layer graphene oxide was finally obtained.

Generation of NGO Patterns

Photoresist (PR) micropatterns were generated on Si wafer using conventional photolithographic technique. PR on Si wafer was further coated with (heptadecafluoro-1,1,2,2-tetrahydrocyclo)trichlorosilane for 3 h in desiccator to prevent a possible damage from PDMS curing and to facilitate the detachment of cured PDMS from the mold. PDMS poured on to the PR-micropatterned silicon wafer was kept in the oven for 6 h for curing. After the PDMS stamp was detached from PR mold, oxygen plasma was treated on PDMS, followed by coating it with NGO solution dissolved in DIW (1.5 mg/mL) three times using spin coater (Laurell Technologies Corp.) with three different parameters for each coating step (200 rpm for 5 s, 500 rpm for 10 s, 1500 rpm for 20 s). Desired substrates (*e.g.*, gold substrate, silicon wafer or cell culture dish) were then treated with oxygen plasma to attract NGO film on the surface of PDMS stamp. Humidifier was utilized to increase the level of humidity which was important for mediating the transfer of NGO pattern to the desired substrates. Pressure was applied (0.79 N) on the PDMS stamp to facilitate the transfer of NGO film to the desired substrate and to increase the adhesion strength of NGO film. Substrates with NGO patterns were finally washed with ethanol and DIW. In the case of generating NGO patterns on PLGA film, NGO patterns were first generated on the Si wafer. Then, 100 μL of a 150 mg/mL PLGA (50:50) dissolved in THF was added dropwise to the Si wafer. After placing under vacuum for 1 h, the PLGA was then peeled to transfer NGO patterns from Si wafer to the PLGA film.

Cell Culture and Differentiation

To culture hADMSCs ($p = 3$), cell culture dish was first coated with fibronectin (0.65 $\mu g/cm^2$) dissolved in HBSS in the incubator for 2 h. TrypLE was used to detach hADMSCs from the cell culture dish. Approximately 45 000 cells were seeded in the 12-well cell culture dish containing the presterilized substrates bearing NGO patterns. After 2 days of cultivation to promote cell attachment and alignment, 0.5% FBS ASC medium was changed

to osteogenic medium containing 100 nM dexamethasone, 50 μ M ascorbic acid and 10 mM β -glycerolphosphate to start osteogenic differentiation of hADMSCs.²⁶ Medium was changed every 5 days during the differentiation. In the case of neurogenesis, the hADMSCs were first induced toward an ectodermal (neural) lineage using a modified media formulation.⁴² Briefly, the hADMSCs were first grown to >90% confluence in 0.5% FBS ASC medium. Half of the cell culture media was then exchanged with neural induction media (NIM) (DMEM-F12, 2% B27, 1% Penicillin/Streptomycin) supplemented with 20 ng/mL epidermal growth factor (EGF), 20 ng/mL basic fibroblast growth factor (bFGF) and 10 ng/mL brain-derived neurotrophic factor (BDNF). The media was then completely exchanged with the growth factor supplemented NIM. After a total of 10 days, the neural-induced hADMSCs were detached using Accutase and seeded on the laminin-coated (10 μ g/mL) substrates. Cells were then cultured in NIM supplemented with FGF and BDNF, and the media was exchanged every 4–5 days.

Fluorescence Imaging

For actin staining of hADMSCs, cells were washed with DPBS (pH 7.4) and fixed with 4% formaldehyde solution for 10 min at room temperature (RT), followed by three times of washing with DPBS. Cells were then treated with 0.1% Triton X-100 in PBS for 5 min, washed with DPBS and stained with Alexa Fluor 546 Phalloidin-containing solution for 20 min at RT. After washing cells with DPBS for two times, actin-stained cells were placed on the slide glass using ProLong Gold Antifade Mountant as mounting solution for fluorescence imaging. For immunofluorescence staining, cell fixation was same as actin staining described as above. After cell fixation, cells were treated with 0.3% Triton X-100 solution containing 10% normal goat serum for 1 h in cell culture hood. Solution containing primary antibody specifically binds to osteocalcin/Tuj1 was applied and kept for 1 h, followed by washing with DPBS. Secondary antibody (anti-mouse IgG) was further applied to tag primary antibody, kept for 1 h and washed with DPBS. Finally, Hoechst (3 μ g/mL) was used to stain nucleus for immunofluorescence imaging (Eclipse Ti-U, Nikon, Japan).

Alkaline Phosphatase and Alizarin Red S Assays

Alkaline phosphatase (AP), an enzyme expressed by cells, is a marker of osteogenic differentiation.³² Cells were assayed using AP at the approximated midpoint in differentiation (D14). Briefly, media was removed and 0.15% Triton-X-100 was added to each chamber. Plates were incubated with shaking for 40 min, followed by addition of *p*-nitrophenyl phosphate (PNPP) to each chamber. The plates were incubated for 30 min in the dark at room temperature and 3 M NaOH was added to stop the reaction. Absorbances were read at 405 nm using Infinite 200 PRO microplate reader (Tecan, Switzerland). For Alizarin Red S assay, cells were washed with DPBS (pH 7.4) and fixed with 4% formaldehyde solution for 10 min at RT, followed by three times of washing with DPBS. After cell fixation, Alizarin Red solution (40 mM, pH 4.2) was added to each well and kept for 30 min with gentle shaking. The pH of Alizarin Red solution was carefully adjusted using pH meter (Accumet Basic, AB15, Fisher Scientific) since pH is critical for calcium staining. Solution was removed and cells were washed with DI water 5 times. Calcium-stained cells were imaged using optical microscope (Eclipse Ti-U, Nikon, Japan). To achieve quantitative results, cells were de-stained using 10% cetylpyridinium chloride (CPC) in 10 mM

sodiumphosphate (pH 7.0) for 30 min at RT. Finally, Alizarin Red S concentration was determined by absorbance measurement at 562 nm on a multiplate reader (Tecan, Switzerland).

Supplementary Material

Refer to Web version on PubMed Central for supplementary material.

Acknowledgments

We thank Anthony Dudzinski, Ruth Goldman, and Michael Moeller (American CryoStem) for providing the ADMSCs and cell medium. J. Choi acknowledges financial support from the National Research Foundation of Korea (NRF) grant funded by the Korea government (MSIP) (No. 2014R1A2A1A10051725). K. Lee acknowledges financial support from the NIH R21 Grant [1R21NS085569-01]. S. Shah acknowledges NSF DGE, Integrative Graduate Education and Research Traineeship (IGERT) on the Integrated Science and Engineering of Stem Cells. The authors acknowledge assistance from Samir Shubeita and Hang Dong Lee for helium ion microscope imaging.

REFERENCES AND NOTES

1. Engler AJ, Sen S, Sweeney HL, Discher DE. Matrix Elasticity Directs Stem Cell Lineage Specification. *Cell*. 2006; 126:677–689. [PubMed: 16923388]
2. Guvendiren M, Burdick JA. Stiffening Hydrogels to Probe Short- and Long-Term Cellular Responses to Dynamic Mechanics. *Nat Commun*. 2012; 3:792. [PubMed: 22531177]
3. Li XM, Liu HF, Niu XF, Yu B, Fan YB, Feng QL, Cui FZ, Watari F. The Use of Carbon Nanotubes to Induce Osteogenic Differentiation of Human Adipose-Derived MSCs *in Vitro* and Ectopic Bone Formation *in Vivo*. *Biomaterials*. 2012; 33:4818–4827. [PubMed: 22483242]
4. Maroof AM, Keros S, Tyson JA, Ying SW, Ganat YM, Merkle FT, Liu B, Goulburn A, Stanley EG, Elefanty AG, et al. Directed Differentiation and Functional Maturation of Cortical Interneurons from Human Embryonic Stem Cells. *Cell Stem Cell*. 2013; 12:559–572. [PubMed: 23642365]
5. Ravichandran R, Venugopal JR, Sundarajan S, Mukherjee S, Ramakrishna S. Precipitation of Nanohydroxyapatite on PLIA/PBLG/Collagen Nanofibrous Structures for the Differentiation of Adipose Derived Stem Cells to Osteogenic Lineage. *Biomaterials*. 2012; 33:846–855. [PubMed: 22048006]
6. Wingate K, Bonani W, Tan Y, Bryant SJ, Tan W. Compressive Elasticity of Three-Dimensional Nanofiber Matrix Directs Mesenchymal Stem Cell Differentiation to Vascular Cells with Endothelial or Smooth Muscle Cell Markers. *Acta Biomater*. 2012; 8:1440–1449. [PubMed: 22266031]
7. Kim TH, Lee KB, Choi JW. 3D Graphene Oxide-Encapsulated Gold Nanoparticles to Detect Neural Stem Cell Differentiation. *Biomaterials*. 2013; 34:8660–8670. [PubMed: 23937915]
8. Shah S, Solanki A, Sasmal PK, Lee KB. Single Vehicular Delivery of siRNA and Small Molecules to Control Stem Cell Differentiation. *J Am Chem Soc*. 2013; 135:15682–15685. [PubMed: 24106916]
9. Solanki A, Shah S, Yin PT, Lee KB. Nanotopography-Mediated Reverse Uptake for siRNA Delivery into Neural Stem Cells to Enhance Neuronal Differentiation. *Sci Rep*. 2013; 3
10. Discher DE, Mooney DJ, Zandstra PW. Growth Factors, Matrices, and Forces Combine and Control Stem Cells. *Science*. 2009; 324:1673–1677. [PubMed: 19556500]
11. Du J, Chen XF, Liang XD, Zhang GY, Xu J, He LR, Zhan QY, Feng XQ, Chien S, Yang C. Integrin Activation and Internalization on Soft ECM as a Mechanism of Induction of Stem Cell Differentiation by ECM Elasticity. *Proc Natl Acad Sci US A*. 2011; 108:9466–9471.
12. Kilian KA, Bugarija B, Lahn BT, Mrksich M. Geometric Cues for Directing the Differentiation of Mesenchymal Stem Cells. *Proc Natl Acad Sci US A*. 2010; 107:4872–4877.
13. Guilak F, Cohen DM, Estes BT, Gimble JM, Liedtke W, Chen CS. Control of Stem Cell Fate by Physical Interactions with the Extracellular Matrix. *Cell Stem Cell*. 2009; 5:17–26. [PubMed: 19570510]

14. Pelham RJ, Wang YL. Cell Locomotion and Focal Adhesions are Regulated by Substrate Flexibility. *Proc Natl Acad Sci US A*. 1997; 94:13661–13665.
15. Solanki A, Shah S, Memoli KA, Park SY, Hong S, Lee KB. Controlling Differentiation of Neural Stem Cells Using Extracellular Matrix Protein Patterns. *Small*. 2010; 6:2509–2513. [PubMed: 20859950]
16. Yao X, Peng R, Ding JD. Cell-Material Interactions Revealed *via* Material Techniques of Surface Patterning. *Adv Mater*. 2013; 25:5257–5286. [PubMed: 24038153]
17. Wang X, Song W, Kawazoe N, Chen G. The Osteogenic Differentiation of Mesenchymal Stem Cells by Controlled Cell-Cell Interaction on Micropatterned Surfaces. *J Biomed Mater Res, Part A*. 2013; 101:3388–95.
18. Dalby MJ, Gadegaard N, Oreffo ROC. Harnessing Nanotopography and Integrin-Matrix Interactions to Influence Stem Cell Fate. *Nat Mater*. 2014; 13:558–569. [PubMed: 24845995]
19. Park SY, Choi DS, Jin HJ, Park J, Byun KE, Lee KB, Hong S. Polarization-Controlled Differentiation of Human Neural Stem Cells Using Synergistic Cues from the Patterns of Carbon Nanotube Monolayer Coating. *ACS Nano*. 2011; 5:4704–4711. [PubMed: 21568294]
20. Peng R, Yao X, Ding JD. Effect of Cell Anisotropy on Differentiation of Stem Cells on Micropatterned Surfaces through the Controlled Single Cell Adhesion. *Biomaterials*. 2011; 32:8048–8057. [PubMed: 21810538]
21. Yan C, Sun JG, Ding JD. Critical Areas of Cell Adhesion on Micropatterned Surfaces. *Biomaterials*. 2011; 32:3931–3938. [PubMed: 21356556]
22. Tay CY, Yu HY, Pal M, Leong WS, Tan NS, Ng KW, Leong DT, Tan LP. Micropatterned Matrix Directs Differentiation of Human Mesenchymal Stem Cells towards Myocardial Lineage. *Exp Cell Res*. 2010; 316:1159–1168. [PubMed: 20156435]
23. Kim DN, Lee W, Koh WG. Micropatterning of Proteins on the Surface of Three-Dimensional Poly(ethylene glycol) Hydrogel Microstructures. *Anal Chim Acta*. 2008; 609:59–65. [PubMed: 18243874]
24. Koh WG, Revzin A, Pishko MV. Poly(ethylene glycol) Hydrogel Microstructures Encapsulating Living Cells. *Langmuir*. 2002; 18:2459–2462. [PubMed: 12088033]
25. McMurray RJ, Gadegaard N, Tsimbouri PM, Burgess KV, McNamara LE, Tare R, Murawski K, Kingham E, Oreffo ROC, Dalby MJ. Nanoscale Surfaces for the Long-Term Maintenance of Mesenchymal Stem Cell Phenotype and Multipotency. *Nat Mater*. 2011; 10:637–644. [PubMed: 21765399]
26. Lee WC, Lim CHYX, Shi H, Tang LAL, Wang Y, Lim CT, Loh KP. Origin of Enhanced Stem Cell Growth and Differentiation on Graphene and Graphene Oxide. *ACS Nano*. 2011; 5:7334–7341. [PubMed: 21793541]
27. Yin PT, Shah S, Chhowalla M, Lee K-B. Design, Synthesis, and Characterization of Graphene-Nanoparticle Hybrid Materials for Bioapplications. *Chem Rev*. 2015; doi: 10.1021/cr500537t
28. Nayak TR, Andersen H, Makam VS, Khaw C, Bae S, Xu XF, Ee PLR, Ahn JH, Hong BH, Pastorin G, et al. Graphene for Controlled and Accelerated Osteogenic Differentiation of Human Mesenchymal Stem Cells. *ACS Nano*. 2011; 5:4670–4678. [PubMed: 21528849]
29. Solanki A, Chueng STD, Yin PT, Kappera R, Chhowalla M, Lee KB. Axonal Alignment and Enhanced Neuronal Differentiation of Neural Stem Cells on Graphene-Nanoparticle Hybrid Structures. *Adv Mater*. 2013; 25:5477–5482. [PubMed: 23824715]
30. Shah S, Yin PT, Uehara TM, Chueng STD, Yang LT, Lee KB. Guiding Stem Cell Differentiation into Oligodendrocytes Using Graphene-Nanofiber Hybrid Scaffolds. *Adv Mater*. 2014; 26:3673–3680. [PubMed: 24668911]
31. Zuk PA, Zhu M, Ashjian P, De Ugarte DA, Huang JI, Mizuno H, Alfonso ZC, Fraser JK, Benhaim P, Hedrick MH. Human Adipose Tissue is a Source of Multipotent Stem Cells. *Mol Biol Cell*. 2002; 13:4279–4295. [PubMed: 12475952]
32. Zuk PA, Zhu M, Mizuno H, Huang J, Futrell JW, Katz AJ, Benhaim P, Lorenz HP, Hedrick MH. Multilineage Cells from Human Adipose Tissue: Implications for Cell-Based Therapies. *Tissue Eng*. 2001; 7:211–228. [PubMed: 11304456]
33. Kane RS, Takayama S, Ostuni E, Ingber DE, Whitesides GM. Patterning Proteins and Cells Using Soft Lithography. *Biomaterials*. 1999; 20:2363–2376. [PubMed: 10614942]

34. Xu YX, Bai H, Lu GW, Li C, Shi GQ. Flexible Graphene Films *via* the Filtration of Water-Soluble Noncovalent Functionalized Graphene Sheets. *J Am Chem Soc.* 2008; 130:5856–5857. [PubMed: 18399634]
35. Peng R, Yao X, Cao B, Tang J, Ding JD. The Effect of Culture Conditions on the Adipogenic and Osteogenic Inductions of Mesenchymal Stem Cells on Micropatterned Surfaces. *Biomaterials.* 2012; 33:6008–6019. [PubMed: 22681981]
36. Trappmann B, Gautrot JE, Connelly JT, Strange DGT, Li Y, Oyen ML, Stuart MAC, Boehm H, Li BJ, Vogel V, et al. Extracellular-Matrix Tethering Regulates Stem-Cell Fate. *Nat Mater.* 2012; 11:642–649. [PubMed: 22635042]
37. McBeath R, Pirone DM, Nelson CM, Bhadriraju K, Chen CS. Cell Shape, Cytoskeletal Tension, and RhoA Regulate Stem Cell Lineage Commitment. *Dev Cell.* 2004; 6:483–495. [PubMed: 15068789]
38. Higuchi A, Ling QD, Chang Y, Hsu ST, Umezawa A. Physical Cues of Biomaterials Guide Stem Cell Differentiation Fate. *Chem Rev.* 2013; 113:3297–3328. [PubMed: 23391258]
39. Kim J, Kim YR, Kim Y, Lim KT, Seonwoo H, Park S, Cho SP, Hong BH, Choung PH, Chung TD, et al. Graphene-Incorporated Chitosan Substrata for Adhesion and Differentiation of Human Mesenchymal Stem Cells. *J Mater Chem B.* 2013; 1:933–938.
40. Park J, Park S, Ryu S, Bhang SH, Kim J, Yoon JK, Park YH, Cho SP, Lee S, Hong BH, et al. Graphene-Regulated Cardiomyogenic Differentiation Process of Mesenchymal Stem Cells by Enhancing the Expression of Extracellular Matrix Proteins and Cell Signaling Molecules. *Adv Healthcare Mater.* 2014; 3:176–181.
41. Park SY, Park J, Sim SH, Sung MG, Kim KS, Hong BH, Hong S. Enhanced Differentiation of Human Neural Stem Cells into Neurons on Graphene. *Adv Mater.* 2011; 23:H263–H267. [PubMed: 21823178]
42. Anghileri E, Marconi S, Pignatelli A, Cifelli P, Galie M, Sbarbati A, Krampera M, Belluzzi O, Bonetti B. Neuronal Differentiation Potential of Human Adipose-Derived Mesenchymal Stem Cells. *Stem Cells Dev.* 2008; 17:909–916. [PubMed: 18564036]
43. Bae KS, Park JB, Kim HS, Kim DS, Park DJ, Kang SJ. Neuron-like Differentiation of Bone Marrow-Derived Mesenchymal Stem Cells. *Yonsei Med J.* 2011; 52:401–412. [PubMed: 21488182]
44. Akhavan O, Ghaderi E. Differentiation of Human Neural Stem Cells into Neural Networks on Graphene Nanogrids. *J Mater Chem B.* 2013; 1:6291–6301.
45. Tang ML, Song Q, Li N, Jiang ZY, Huang R, Cheng GS. Enhancement of Electrical Signaling in Neural Networks on Graphene Films. *Biomaterials.* 2013; 34:6402–6411. [PubMed: 23755830]
46. Das KP, Freudenrich TM, Mundy WR. Assessment of PC12 Cell Differentiation and Neurite Growth: A Comparison of Morphological and Neurochemical Measures. *Neurotoxicol Teratol.* 2004; 26:397–406. [PubMed: 15113601]
47. Zhu YW, Murali S, Cai WW, Li XS, Suk JW, Potts JR, Ruoff RS. Graphene and Graphene Oxide: Synthesis, Properties, and Applications. *Adv Mater.* 2010; 22:3906–3924. [PubMed: 20706983]
48. Hu X, Park SH, Gil ES, Xia XX, Weiss AS, Kaplan DL. The Influence of Elasticity and Surface Roughness on Myogenic and Osteogenic-Differentiation of Cells on Silk-Elastin Biomaterials. *Biomaterials.* 2011; 32:8979–8989. [PubMed: 21872326]
49. Palchesko RN, Zhang L, Sun Y, Feinberg AW. Development of Polydimethylsiloxane Substrates with Tunable Elastic Modulus to Study Cell Mechanobiology in Muscle and Nerve. *PLoS One.* 2012; 7

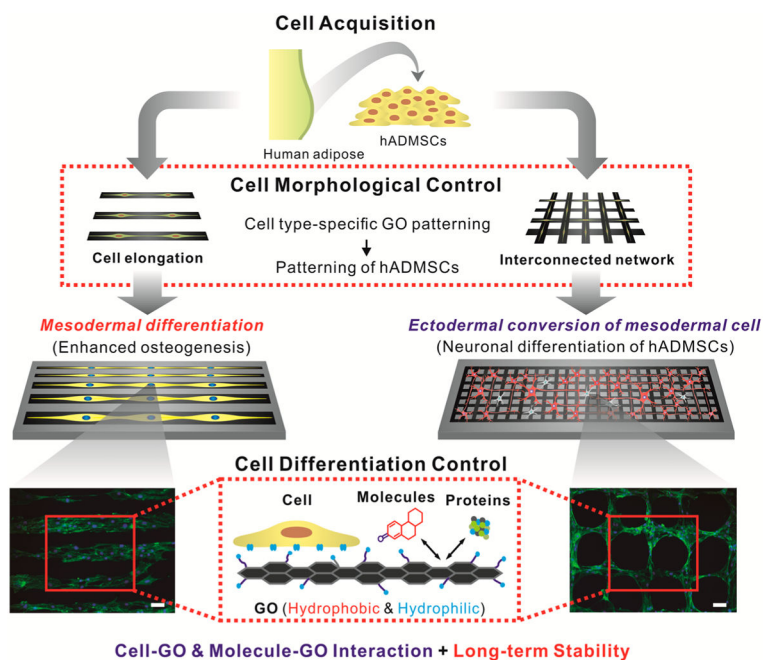


Figure 1. Schematic diagram illustrating control over the differentiation of adipose-derived stem cells using combinatorial graphene hybrid-pattern arrays. The scheme represents the steps taken to modulate the morphology of hADMSCs (adipose tissue from 29- and 63-year-old-female patients) using NGO patterns and to guide differentiation based on the physico-chemical characteristics of NGO. This method resulted in enhanced differentiation into osteoblasts and neurons in a selective and efficient way. Fluorescence images shown are F-actin-stained hADMSCs whose morphologies were controlled by NGO line and grid patterns in combination with PEG-containing passivation molecule. Scale bar = 100 μm .

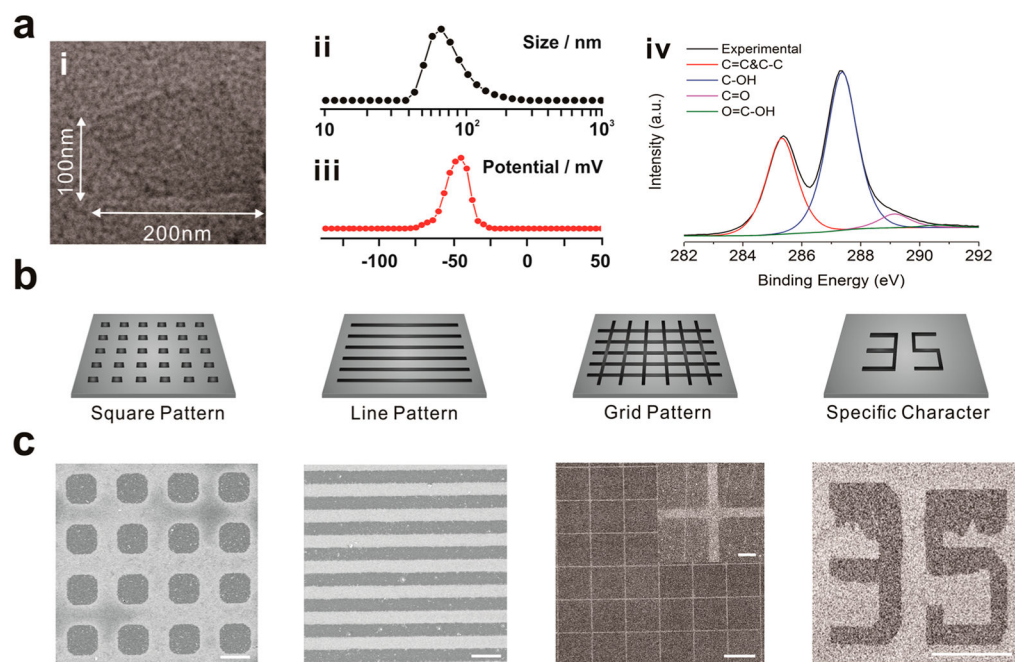


Figure 2. Combinatorial graphene pattern arrays with different geometries. (a) (i) TEM image, (ii) size distribution, (iii) zeta potential, (iv) XPS analysis of NGO used in this study. (b) Schematic diagram of NGO micropatterns and (c) the corresponding NGO patterns (squares, lines, grid and numbers) generated on the Au/glass substrates were visualized by helium ion microscopy (HIM). Scale bars are $5 \mu\text{m}$ for squares and lines, $100 \mu\text{m}$ for grid and character, and $10 \mu\text{m}$ for inset image of grid pattern, respectively.

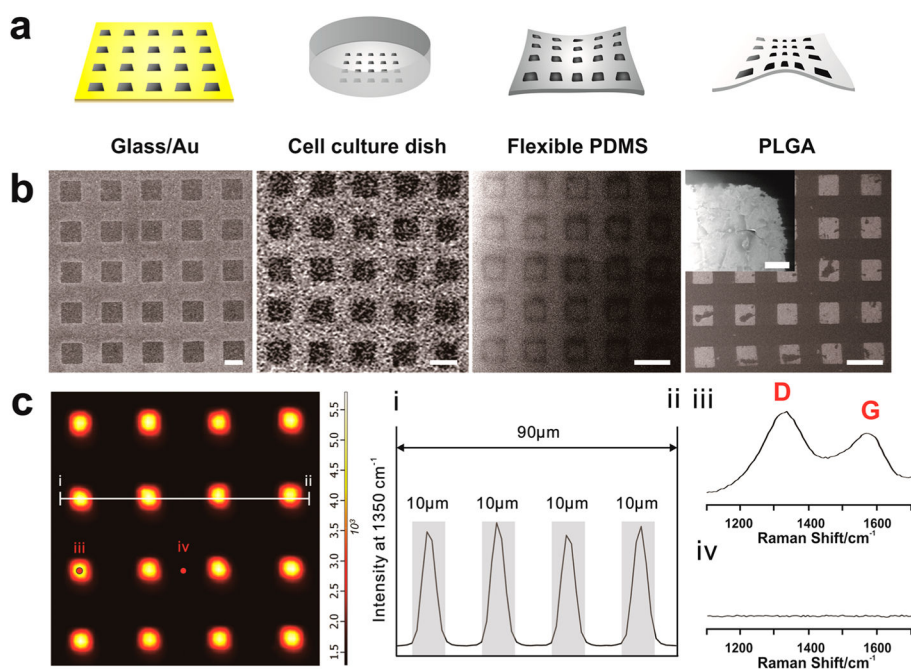


Figure 3. Combinatorial graphene pattern arrays on different substrates. (a) Schematic diagram representing four different types of biocompatible substrates (Au-deposited glass, TCP, flexible PDMS and poly(lactic-*co*-glycolic acid) (PLGA)) having NGO square patterns on its surface. (b) Helium ion microscopy (HIM) images of NGO square patterns generated on Au-deposited glass, TCP, flexible PDMS and PLGA that match with the illustrations represented in (a). Scale bar = 20 μm . Inset is the high magnification image of NGO pattern on PLGA that shows detailed features of NGO pattern. Scale bar = 500 nm. (c) Confocal Raman mapping image of NGO square pattern generated on the glass/Au substrate, using D band (1350 cm^{-1}) of graphene oxide as an indicator for the Raman intensities. The X and Y axes were $100\ \mu\text{m} \times 100\ \mu\text{m}$. (i and ii) Intensity profile of Raman peak (D band of GO) that shows the size of NGO patterns (10 μm). Gray color represents the region that shows strong Raman peaks assigned to D band, which matches with the size of NGO pattern. Raman spectra obtained from the spot (iii) and (iv) from the Raman mapping image that proves the presence and absence of NGO based on strong D and G band. Detection time was 5 and 20 s for mapping image and Raman spectra shown in (iii) and (iv), respectively.

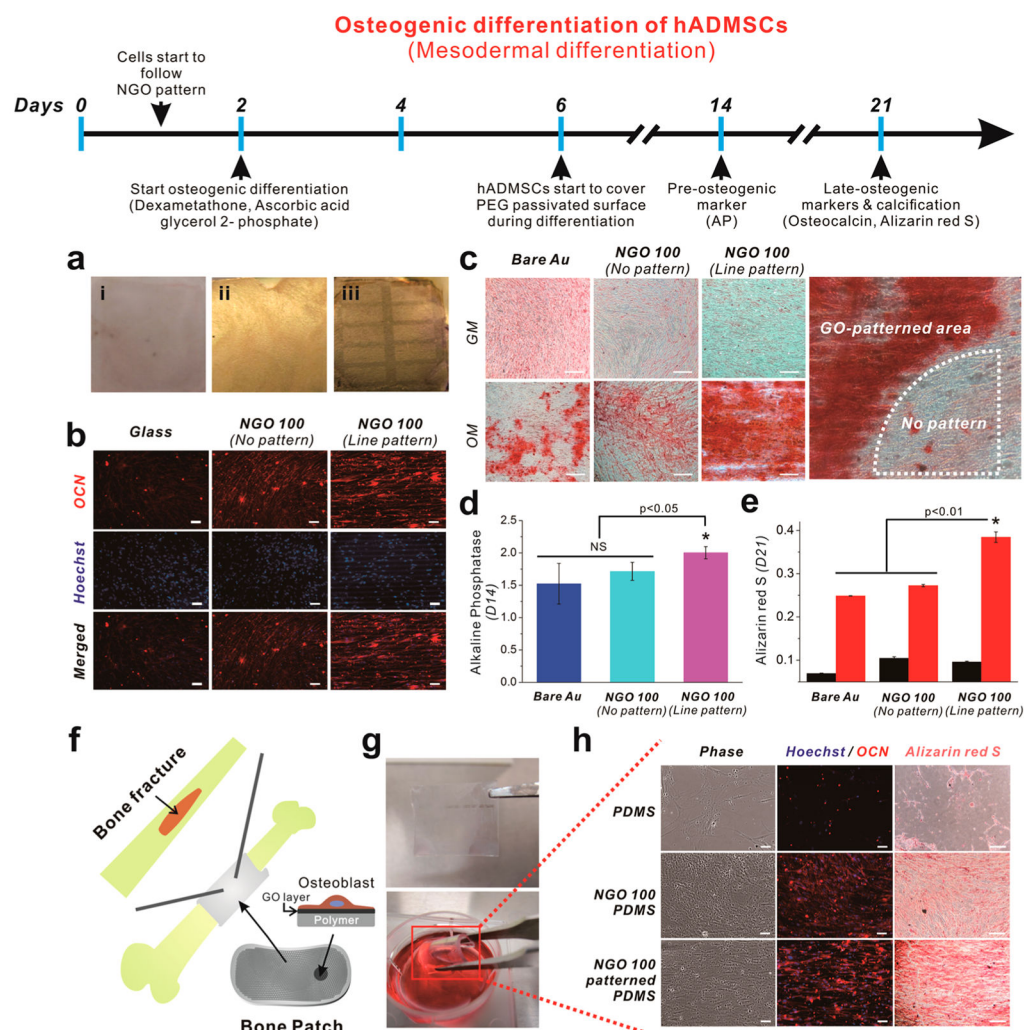


Figure 4. Osteogenic differentiation of hADMSCs using NGO line-patterned substrate. (a) Picture of (i) glass, (ii) NGO-coated gold substrate, and (iii) NGO line-patterned substrate used for the osteogenesis of hADMSCs for 3 weeks, showing ultimate stability of NGO line pattern generated on the substrate. (b) Fluorescence images of hADMSCs differentiated into osteoblasts stained for osteocalcin (red, top row), nucleus (blue, middle row) and merged (last row), showing elongated and well-spread morphology of hADMSCs that directly followed the geometry of NGO line pattern, which are different from the same cells on glass or NGO-coated substrates. NGO line pattern is clearly visible in Hoechst-stained images in the middle row. Scale bar = 50 μm . (c) Differentiated osteoblasts stained with Alizarin red S at day 21 to confirm the level of calcification (red color) from the cells on bare Au, NGO-coated substrate and the substrate with NGO line pattern. GM and OM mean growth medium and osteogenic medium, respectively. “No pattern” means the area which is not covered by NGO line pattern due to the incomplete transfer of NGO on the surface. Scale bar = 50 μm . (d) Alkaline phosphatase (AP) assay to confirm the expression of preosteogenic marker which is dependent on the type of the substrates. (e) Quantitative

analysis of calcium expression of cells treated with GM (black) and OM (red) obtained by extracting Alizarin red S. Results are medians of absorbance signals (460 and 560 nm for AP and Alizarin red S, respectively) obtained from three independent experiments $n = 3$; * $p < 0.05$ or $p < 0.01$, Student's t -test. "NS" indicating that the two groups were not significantly different at $p = 0.05$). (f) Schematic illustration showing possible application of proposed "Bone Patch" composed of supporting polymer (PDMS, Young's modulus: 6.2 MPa), NGO-patterned layer and the osteoblasts derived from hADMSCs from the patient suffering bone fracture. (g) Picture of highly flexible bone patch having NGO pattern and the differentiated osteoblasts. (h) Cells stained for osteocalcin (OCN, red), nucleus (blue) and calcium (Alizarin red S, red) to confirm the successful differentiation into osteoblasts. Scale bar = 50 μm .

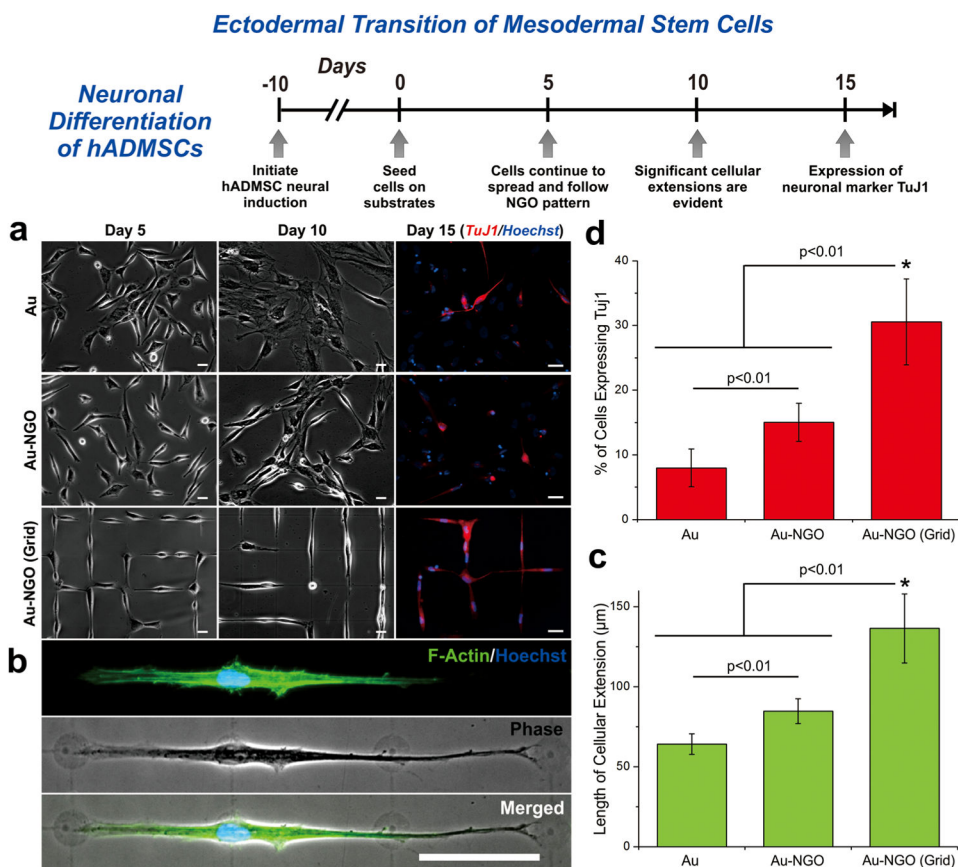


Figure 5. Neuronal differentiation of hADMSCs using NGO grid-patterned substrate. (a) Images of neural induced hADMSCs grown on PLL-coated Au [Au], NGO-coated Au [Au-NGO], and NGO grid-patterned substrates [Au-NGO (Grid)]. All substrates were coated with laminin to facilitate cell attachment. Cellular growth and morphology were monitored over 15 days, followed by staining for the neuronal marker TuJ1 (red) and nucleus (blue). Scale bars = 20 μm . (b) Phase contrast and fluorescence images of cells stained for F-actin (green) and nucleus (blue) after 15 days of cultivation show extensive cellular extension on NGO-grid patterns. Scale bar = 50 μm . (c) Quantitative comparison of the length of cellular extension on various substrates ($n = 3$; $*p < 0.01$, Student's unpaired t test). (d) Quantitative comparison of the percentage of cell expressing the neuronal marker TuJ1 on various substrates ($n = 3$; $*p < 0.01$, Student's unpaired t test).